Dual-Radio Configuration for Flexible Communication in Flocking Micro/Miniature Aerial Vehicles

Andrew Bingler and Kamran Mohseni, *Member, IEEE*

***Abstract*—This paper presents an overview of a new dual-radio autopilot and ground station platform used in hierarchical, micro aerial vehicle flocks to improve communication flexibility and performance. Flocks of micro/miniature aerial vehicles flying in close proximity are often used in scenarios of hazard detection and tracking. Micro aerial vehicle's small size grants a number of benefits, such as improved maneuverability and reduced cost, but also results in sometimes severe resource constraints. To help alleviate these restrictions, as well as to improve overall communication flexibility, this paper proposes the use of a hierarchical, dual-radio autopilot flock configuration. Interflock communication is facilitated by low-power radios, whereas an elected flock leader relays important communications to a ground station via a long-range, high-power radio. Additionally, the diversity provided by the dual-radio system provides inherent redundancy while improving flock communication adaptability for varying data sizes and transmit distances. An energy efficiency model for this dual-radio configuration is also presented and verified by autonomous, multi-vehicle flight tests.**

***Index Terms*—Aerospace electronics, autonomous systems, communication systems, communications technology, cooperative systems, energy efficiency.**

I. Introduction

MICRO/MINIATURE aerial vehicles (MAVs) are a class of unmanned aerial vehicle (UAV) with significant size and weight constraints (see Fig. 1). This size restriction confers a number of benefits, such as reduced costs, improved maneuverability in urban spaces, and other constricted environments, and reduced risk to humans in the event of a crash. Due to this skill set, MAVs are now quite prominent in military, scientific, and civil fields.

An MAV's small size and portability likewise makes them strong candidates for use in collaborate flocks, enabling sensor coverage over large airspaces by forming aerial wireless sensor networks (AWSNs). AWSNs have grown increasingly popular, leading to applications, such as pollutant monitoring, disaster management, and assisting in military operations [1]–[7]. Currently, many AWSN flocks are composed of larger UAVs, which can support extensive payloads and maintain flight for extended periods. Less research has been conducted using MAVs within AWSNs, which, due to their small size, often face greater restrictions in terms of flight time and payload complexity. We have considered some of the unique advantages MAVs offer to carry out research in scenarios of plume detection [3], [8]–[10], such as atmospheric flow sensing [11] and hurricane tracking [2]. Furthermore, we expect future scenarios to require coverage across kilometers of land, such as when tracking multiple plumes in an area or when surveying multiple disparate locations. A single flock may be expected to split into multiple groups of vehicles, each of which could then be separated from one another by significant distances, a configuration that requires more flexible communication than most MAV systems can provide. Additionally, to achieve low costs and turnaround times, many MAVs use inefficient and capability-limited, but economical and easily available communication hardware.

Fig. 1. SWAMP MAVs developed in our group.

Common single-radio systems only partially address some of these concerns. The capabilities of the chosen radio set rigid constraints for what kind of communication is possible, so that tradeoffs between transmit range, data rates, and energy consumption must all be accounted for. Depending on the application, MAVs may need to transmit vastly different amounts of data. Scenarios such as aerial surveillance may only require a small number of frames per second (FPS) of low quality or standard definition video transmission, whereas an MAV tasked with construction or building inspection may need to transmit

Manuscript received January 7, 2018; revised June 26, 2018; accepted August 21, 2018. This work was partially supported in part by the U.S. Air Force Office of Scientific Research and in part by the U.S. Office of Naval Research. *(Corresponding author: Kamran Mohseni.)*

A. Bingler is with the Institute for Networked Autonomous Systems and the Department of Electrical and Computer Engineering, University of Florida, Gainesville, FL 32611 USA (e-mail: abingler@ufl.edu).

K. Mohseni is with the Institute for Networked Autonomous Systems, the Department of Mechanical and Aerospace Engineering and the Department of Electrical and Computer Engineering, University of Florida, Gainesville, FL 32611 USA (e-mail: mohseni@ufl.edu).

Digital Object Identifier 10.1109/JSYST.2018.2867852

an increased number of FPS of high-definition video so that fine-grained details within the environment can be observed.

Data transmission rates then fundamentally come down to how much bandwidth is available on a signal, with higher frequencies capable of supporting larger bandwidths [12]. The 5-GHz band currently supports one of the highest capacity data rates, with a theoretical limit of up to 7 Gb/s when using the 802.11ac protocol [13]. But, higher frequencies attenuate faster and have less penetration through surfaces, such as trees or buildings due to their smaller wavelengths, significantly impacting their range. Slower carrier frequencies, such as the 900-MHz and 1.2-GHz bands, cannot support as much data throughput, but are capable of achieving longer ranges. The LoRa protocol, which commonly operates around the 900-MHz carrier frequency, offers very long ranges (10 to 15 km) at very low powers (current consumption of 10 to 30 mA) [14]. But LoRa is only capable of transmitting a few thousand bytes per second, sufficient only for smaller payloads.

Furthermore, increasing the power of a signal can be used to improve its range. Radios expected to communicate over long distances will require higher transmit powers, and thus larger energy consumption, whereas this energy is wasted when communicating with targets deep within transmit distances. Finally, these single-radio systems are sensitive to hardware failure, such that radio loss on a sensing node obstructs all communication to and from that node.

Motivated by these issues and constraints, we offer the solution of using a dual-radio autopilot system for low-resource and flexible communication. These systems could support two distinct radios, each on a different carrier frequency, alleviating some of the previous data, power, and range constraints. With this added diversity, a vehicle could communicate with multiple targets of different frequencies simultaneously, or aggregate data rates by communicating with one target using both radios. Radio selection could also be updated as needed to suit the application. A vehicle that must transmit a video feed to a nearby ground station while communicating with another target hundreds of meters away may pair a short range, high-throughput radio with a long-range, low-throughput radio.

To better capitalize on these advantages, we propose a dual-radio flock configuration (see Fig. 2), in which each node of a flock is equipped with a long-range and short-range radio. All nodes within the flock act as sensory nodes, collecting environmental data that must be transmitted to a ground station. When within short-range radio distance of a ground station, members of the flock will transmit data directly via short-range radio. When the flock is outside short-range communication, it adopts a hierarchy and elects its most central member as the leader node. All sensor data are then transmitted to this leader node along short-range radio, which relays each node's data payload, along with its own, to the ground station via long-range radio. The role of leader may change between members at any time, such as when the battery of the current leader starts to run low or if a leader vehicle encounters a system failure.

Compared to a standard vehicle flock where each node is equipped with only a long-range radio, we expect a noticeable increase in power efficiency, primarily due to the dual radio, follower nodes placing their long-range radios into a low-power sleep state, whereas a standard single-radio flock must keep its radios idling. This is because at any point, a node in the flock may need to receive important data, which could arrive without prior notice. In flocks composed of single-radio nodes, sleeping a radio is essentially closing that node to all communication.

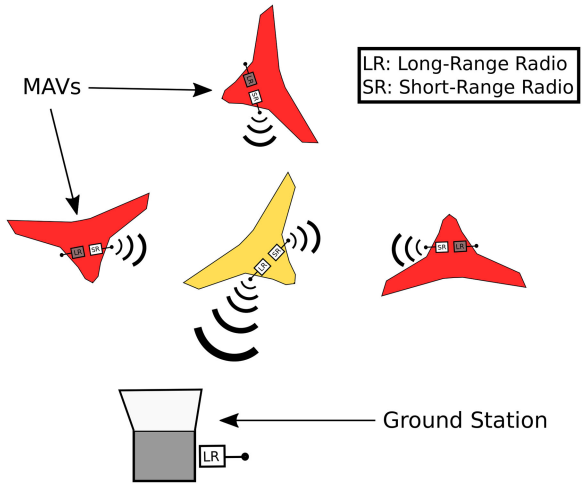

Fig. 2. Visualization of the dual-radio flock scenario. The follower nodes (red) transmit important data to the leader node (yellow) via short-range radio, whereas their long-range radios maintain a low-power sleep state. The leader node collects follower data over short-range radio and retransmits this to the ground station via long-range radio. This networking capability is essential to multi-agent applications, such as cooperative localization [15], [16] or control [17].

Propulsion and wireless communications are the main sources of energy usage for these battery-constricted MAVs [18], and while propulsion can consume much more power than communication, it is still very important to focus on radio energy efficiency. This is because in many applications of fixed-wing vehicles, the vehicle may spend a significant portion of its flight envelope gliding or cruising, during which the motor is not run at full throttle and power consumption of the wireless communications would have a more significant impact on overall power consumption. Because of this, the percentage ratio of communication power to propulsion could be anywhere from 0% to 100% and over depending on the specific flight or mission. For instance, if there is a uniform background flow at sufficient velocity, then an aircraft expected to perform station keeping while communicating could glide within this background flow with its engines off. Furthermore, for vehicles in the range of 50 g, such as the new short wing aerodynamics modeling platform (SWAMP) MAVs developed by our group (see Fig. 1), one does not expect this vehicle to fight background flow using propulsion energy, but instead to "ride" the flow, thereby conserving energy [2]. Otherwise, if an aircraft is required to climb at high rates in an adversarial background flow, then the power consumption will be dominated by the propulsion energy. Thus, due to this chance that wireless communication could consume a significant portion of the node's power, we hope that by improving radio energy efficiency, we can allow these vehicles to operate for longer and dedicate more power to sensing.

To validate our dual-radio flock configuration and address these communication issues, we have designed a new autopilot system, called the autonomous MAV pilot, or AMP [19]. The

AMP is a small, lightweight platform that is designed for research and development, and is capable of flying the SWAMP MAVs (see Fig. 1) developed by our group. We have also designed a novel, dual-radio ground station board, specifically created for interacting with dual-radio flocks.

This manuscript is organized as follows. First, we review the background and related works for this field in Section II. Then, the autopilot system and ground station platform used for experimental testing of the dual-radio MAV flock are presented in Section III. Next, the theoretical model used to estimate the energy consumption of the flock is proposed in Section IV. Following this, the procedures and results of multiple dual-radio flight tests are detailed and compared to our proposed model in Section V. Finally, Section VI provides a discussion of the flight test results and closing considerations.

II. Related Works

In previous research, the use of two or more radios on the nodes of stationary or slow moving wireless sensor networks has shown a number of benefits. Some efforts have focused on using the multi-radio nodes to remove or reroute networking congestion so as to improve data throughput and reduce packet delays [20]–[24]. In such designs [20], lower power radios may always be ON, maintaining a constant network, whereas high-powered radios can be used as needed to assist in data transfer for sinks that show signs of high traffic. In other networks, such as [21], Ji *et al*. take advantage of a dual-radio nodes ability to act in full-duplex [25], receiving and transmitting data simultaneously over different channels. Furthermore, some works [24] focus on supplementing single-radio node networks with dual-radio nodes, which balance the energy consumption per bit between their high- and low-power radios to obtain high-throughput, energy-efficient data transfers. Other configurations may operate two characteristically similar radios to achieve higher aggregate data transfer rates, such as one method [26] that increased data rates by a factor of 3.7 by not only doubling standard throughput, but also by smartly rerouting congestion between the two radios.

Multiple efforts focus on utilizing dual-radio configurations to improve energy efficiency of static or gradually moving networks. Some systems use wake-on-wireless approaches [23], [27]–[29], which use secondary, low-power radios to wake the high-power radio as needed. The method found in [30] uses a high- and low-power radio to physically separate the control channel from the data channel. Control is implemented using the low-power radio, which sends a wakeup message to the device when receiving an incoming call. On wakeup, the high-power radio is used to transmit and receive data. This improves the battery lifetimes of these devices by reducing idle power, as the high-power radio is turned OFF until a wakeup call is received, and instead the low-power radio is left idle for simple reception and wakeup.

Some designs use dual-radios to improve the energy efficiency of very high-throughput network backbones. By equipping nodes of the network with both a high-power, long-range radio and a low-power, short-range radio, the increased flexibility in wireless connectivity reduces overall power consumption [31]. Dual-radio nodes have also been used for emergency signaling, providing a low-power method for real-time communication during emergencies [32].

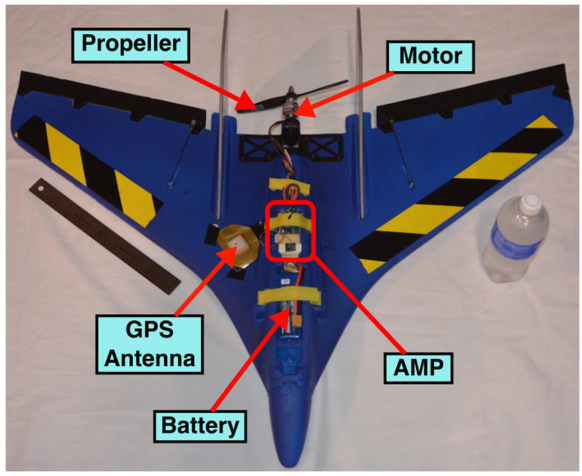

Fig. 3. Delta Wing outfitted with an AMP board, developed by the authors. Both are used and manufactured within our group [2], [8], [19], [33], [34].

Whereas much of the previous research on dual radios has focused on stationary or slow moving networks, such as those created by cellphones, our proposed use of dual-radio nodes is implemented on a fast mobile network of aerial vehicles. Due to this, network topology can change quite rapidly, so communication benefits from both radios being kept at their maximum transmit power, to ensure coverage of all the vehicles in a flock.

III. Experimental Setup

In this section, a description of the experimental setup used to test our dual-radio flock scenario and model is presented. This setup consists of our AMP autopilot system and ground station platform. All flights were conducted on our 0.94-m span Delta Wing aircrafts (see Fig. 3) manufactured and used by our group for environmental monitoring applications [33].

A. AMP Autopilot

The AMP is a dual-radio autopilot designed by our group to process data from a suite of onboard sensors, execute control code, and transmit all pertinent information to a data sink in a manner that is flexible and resource efficient [19]. The AMP's main components (see Fig. 4) include the following:

1) the Microchip dsPIC33EP512GM306 processor;
2) the InvenSense MPU9250 nine-axis IMU;
3) the Bosch BMP180 pressure sensor;
4) the Sensirion SHT25 humidity sensor;
5) the Linx TM GPS receiver;
6) the Digi Series 1 XBee-PRO radio;
7) the Cypress CYRF6936 radio;
8) the TI INA226 power monitor;
9) a 3.3-V regulator;
10) ports for interfacing with external sensors, servos, and radios.

The AMP is composed of two boards: the main board and the sensor breakout board [see Fig. 5(a) and (b)]. The main

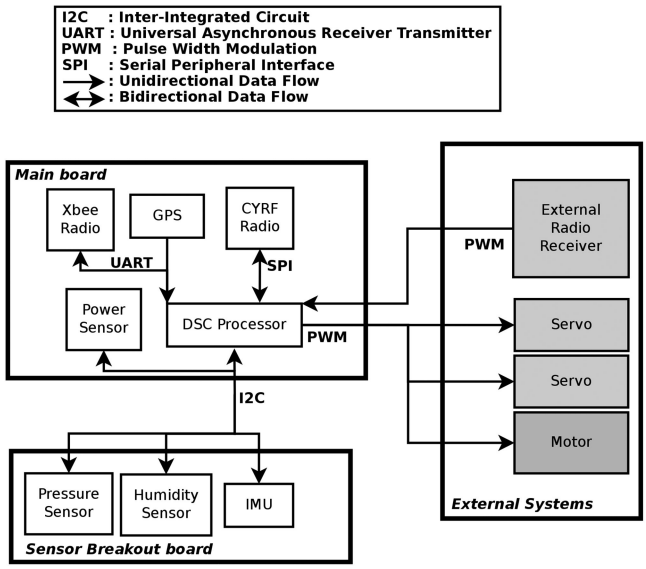

Fig. 4. Block diagram of the AMP autopilot created and designed by the authors [19]. The AMP is divided between three systems, the main board, the sensor breakout board, and the external hardware. Communication methods and data directionality are indicated.

board acts as the central hub for the AMP, connecting the various elements of communication, sensing, and control together. The main board includes a development port, joining a number of processor peripherals to user accessible pins, as shown in Fig. 5(b). This allows the AMP to be used as a rapid development tool, providing access to the interintegrated circuit and serial peripheral interface communication protocols, pulsewidth modulation output, or analog-to-digital conversion features of the processor. As a result, future components, such as new or upgraded sensors, may be added without requiring a new revision of the board. The INA226 current shunt and power monitor is a recent addition to the AMP and enables monitoring of the autopilot's power consumption.

The sensor breakout board is designed to house the majority of the MEMS sensors used by the AMP. Confining sensor placement to the sensor breakout board provides a number of benefits. The pressure and humidity sensors used by the autopilot are sensitive to ambient temperature, so by separating them from the main board, interference from heat producing components (such as the GPS or processor) can be kept to a minimum. The small size of the sensor breakout also creates more options with regard to placement of the board on or within the body of a vehicle, as compared to the larger main board. For instance, the SHT25 requires exposure to the airflow of which humidity is to be measured. Thus, the sensor breakout can be affixed to the exterior of a vehicle to satisfy this requirement.

The XBee and CYRF6936 are the long- and short-range radios for the AMP, respectively. Transmit power specifications for the CYRF and XBee are shown in Tables I and II, respectively. Transmit power values for the CYRF were taken from the CYRF6936 datasheet [35], whereas XBee power values were measured, as they are not provided within the datasheet [36].

TABLE I
TRANSMIT POWER TO CURRENT SPECIFICATIONS FOR THE CYRF6936 (SYSTEM VOLTAGES OF 3.3 V)

Power (dBm)	Current (mA)
-35	15.5
-30	15.8
-24	16.45
-18	17.3
-13	18.5
-5	21.55
0	27.2
4	36.75

TABLE II
TRANSMIT POWER TO CURRENT SPECIFICATIONS FOR THE XBEE (SYSTEM VOLTAGES OF 3.3 V)

Power (dBm)	Current (mA)
10	126.5
12	146.9
14	163.6
16	181.9
18	216.3

These measurements were taken using the INA226 while the XBee was transmitting at each of its five transmit power levels. To reduce interference between the two radios, the CYRF operates at a 2.472-GHz carrier frequency, whereas the XBee operates at 2.417-GHz. Both radios are equipped with omnidirectional whip antennas. When used in a flock, communication between AMPs is handled synchronously, using a form of time division multiplexing, where each autopilot is allocated a time slot during which time it can communicate.

B. Ground Station

Our system's ground station consists of a laptop running a MATLAB GUI, connected to XBee and CYRF radios via USB. The ground station's design focuses on presenting any relevant user information, in a way that is quick, clear, and efficient. The ground station also allows the user to easily uplink data to one or more autopilots, such as for updating control variables or flight coordinates. Otherwise, configuring an autopilot or setting flight controls could be burdensome.

A new ground station board has also been designed by the authors. Called the supervisor board (or SuperBoard), it was created specifically for interacting with our dual-radio autopilot system [see Fig. 6(a) and (b)]. The SuperBoard allows us to facilitate communication with both radios and improve the overall communication capabilities of the AMP. The main components of this board (see Fig. 7) include the following:

1) the Microchip dsPIC33EP512GM306 processor;
2) the Digi Series 1 XBee-PRO radio;
3) the Cypress CYRF6936 radio;
4) the FT232 FTDI chip.

The SuperBoard provides a number of advantages. First, it allows us to interact with the CYRF6936 chip over USB, as USB CYRF6936 transceiver units are not widely available. Second, data flow is more easily managed by passing all ground station communications through a single interface, which also improves

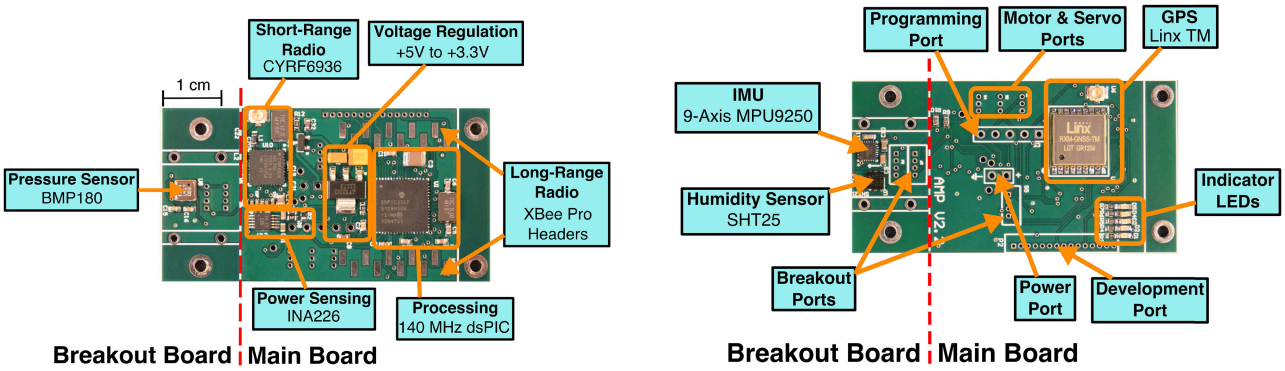

Fig. 5. (a) Bottom and (b) top views of the AMP board, developed by the authors [19]. The processor, CYRF radio, XBee headers, voltage regulator, pressure sensor, GPS, IMU, humidity sensor, ports, LEDs, and separation line between the main and breakout boards are indicated.

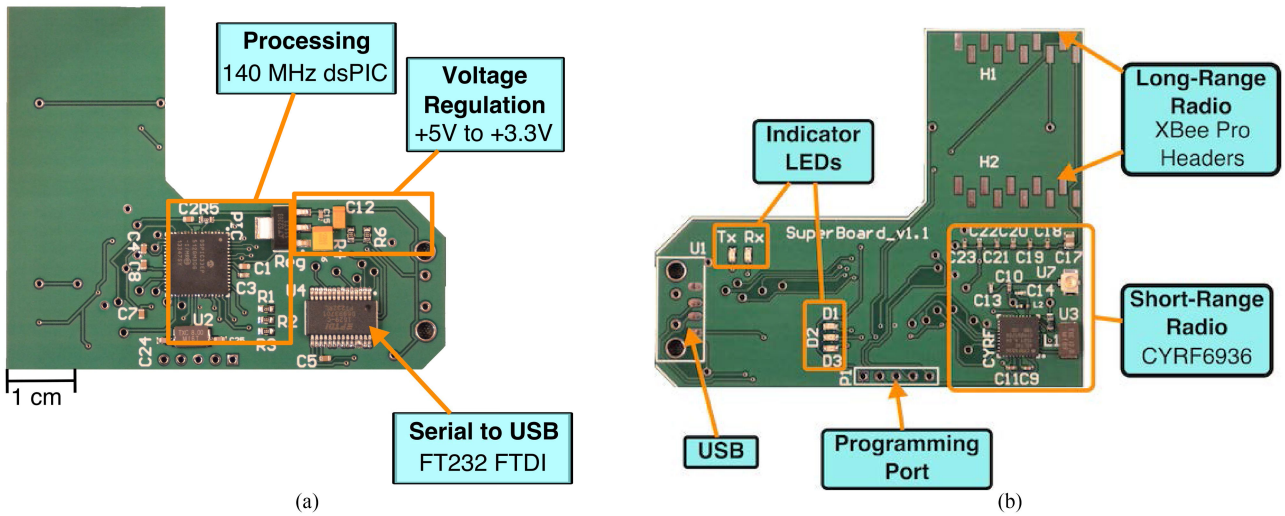

Fig. 6. (a) Bottom and (b) top views of the SuperBoard, developed by the authors. The processor, voltage regulator, FTDI chip, CYRF radio, XBee headers, ports, and LEDs are indicated.

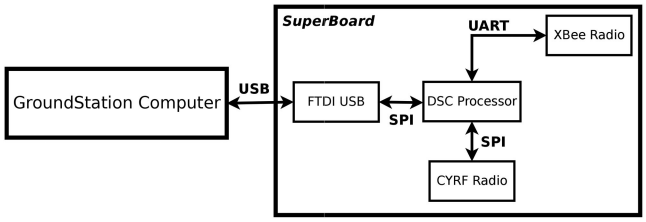

Fig. 7. Block diagram of the SuperBoard ground station designed by the authors. All data flow between the computer and radios is bidirectional. Communication methods are indicated.

compatibility with MATLAB. Third, using the SuperBoard's included processor, we can smartly route or preprocess the incoming or outgoing data flow (such as for error handling or packet filtering).

IV. Dual-Radio Model

In our dual-radio model, a flock is composed of n vehicles, where $n \geq 2$, and each vehicle acts as a sensing node equipped with two radios: A short-range radio and a long-range radio. For data collection, all nodes need to directly or indirectly communicate with one or more ground stations.

If any members of the flock are within short-range communication of the ground station, then messages are transmitted over short-range radio directly to the ground station. Otherwise, the flock elects a member as the leader node. To choose this leader, each MAV broadcasts a data packet containing their identifier and GPS location over short-range radio. Each member then compares the received location data to determine which MAV is most central, and thus should be elected leader. Following this, the elected leader broadcasts an acknowledgment of its new role. This leader node then relays communications from the remaining flock (via short-range radio) and itself to the ground station using its long-range radio. To conserve power, all follower nodes keep their long-range radios in a low-power sleep state.

To build this model, the energy consumption per unit time for the transmit, receive, and idle states must be known. Most radios will list these specifications in their datasheets, however, if they are not listed, or a theoretical radio is to be used, then the transmit power can be estimated by using the power to distance

components of the Friis transmission equation [37]. Let P_t and P_r be the power transmitted and received in dBm, respectively. We can then relate the two with the following:

$$P_r = P_t + D_t + D_r + 20\log_{10}\left(\frac{\lambda}{4\pi d}\right) - F \tag{1}$$

where D_t and D_r are the antenna directivities in dBi of the transmitting and receiving antennas, respectively, F is the fade margin in dBm, λ is the wavelength of the carrier signal in meters, and d is the distance between antennas in meters. λ can also be represented as the ratio of the speed of light c to the carrier signal f as $\lambda = \frac{c}{f}$.

Relating transmission distance and transmit power, the values for D_r, D_t, λ, and P_r are assigned with characteristics from the radio and the antennas used. For example, the CYRF6936 radio [35] has a P_r of -97 dBm, a λ of 125 mm, and the D_r and D_t of the CYRF antennas are 3 dBi.

Finally, a fade margin is subtracted from the equation to account for the non-idealities of transmitting across air. Common fade margin values in the 2.4-GHz carrier frequency range from 10 to 30 dBm [38]. With all other constants assigned, (1) can be rearranged to solve for either transmit power or distance.

A note on the values for transmit power. For (1), transmit power is in dBm, but this can be converted to milliwatts by using the following:

$$P_t(\text{mW}) = 1\,\text{mW} \times 10^{\frac{P_t\,(\text{dBm})}{10}}. \tag{2}$$

However, users should be aware that due to the manufacturing constraints and non-idealities of radios, there is a large discrepancy between the transmit power required on the antenna (as derived from (1)) and the power consumed to generate this transmit power (as measured or listed in a radio datasheet). For instance, the CYRF6936 requires 121.3 mW at 3.3 V to generate 2.51 mW (4 dBm) of transmit power. As such, if we want to simulate values based on the distance or other characteristics from (1), then we must first account for this difference. Otherwise, we are limited to the few discrete data points listed in a datasheet or measured from a radio. We do this by fitting the radio transmit power and power consumption to a cubic polynomial model (see [39] and [40])

$$P_t(\text{mW}) = C_1 \cdot x^3 + C_2 \cdot x^2 + C_3 \cdot x + C_4. \tag{3}$$

Now, using values from a datasheet or (1), we can define the power requirements for our short- and long-range radios. First, nondimensionalizing, we substitute our radio-specific power P with P^* where $P^* = \frac{P}{P_c}$ and P_c is a reference value (e.g., P_c is assigned the CYRF transmit power of 36.75 mA at 3.3 V, taken from the CYRF6936 datasheet [35]). P_t^{*s} and P_t^{*l} then represent the energy consumed per unit time transmitting from one node to another over short-range and long-range radios, respectively. P_r^{*s} and P_r^{*l} represent the energy consumed per unit time receiving for a single node over short-range and long-range radios, respectively. Finally, P_{tdl}^{*s} and P_{rdl}^{*s} represent the power consumed for the short-range radio idling in a transmit or receive state, respectively, and P_{tdl}^{*l} and P_{rdl}^{*l} represent the power consumed for the long-range radio idling in a transmit or receive state, respectively. From this, we can create an equation

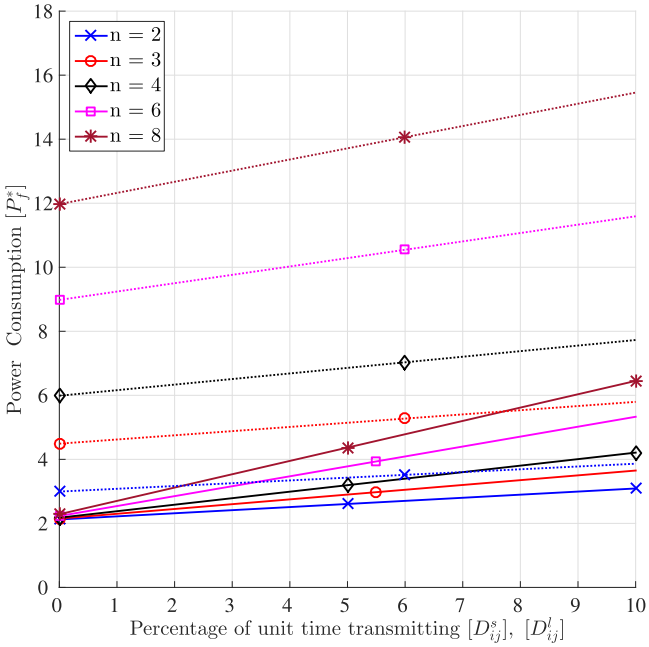

Fig. 8. Simulated power consumption of a flock of AMP autopilots using the dual-radio flock configuration (solid line) and a standard single-radio configuration (dotted line) for several cases. The CYRF and XBee are set to transmit powers of 4 and 18 dBm, respectively.

to determine the total energy of the flock per unit time of data transmitted P_f^*

$$P_f^* = \sum_{i=1}^{n} \left(D_{ij}^s \cdot P_t^{*s} + D_{ij}^s \cdot P_r^{*s} - D_{ij}^s \cdot P_{\text{tdl}}^{*s} - D_{ij}^s \cdot P_{\text{rdl}}^{*s} + D_{ij}^l \cdot P_t^{*l} - D_{ij}^l \cdot P_{\text{tdl}}^{*l}\right) + (n-1) \cdot P_{\text{tdl}}^{*s} + P_{\text{rdl}}^{*s} + P_{\text{tdl}}^{*l} \tag{4}$$

where D_{ij}^s and D_{ij}^l are the percentages per unit time transmitting/receiving data per node i to/from node j, for the short-range and long-range radios, respectively. In cases where $i = j$, then D_{ij}^s and D_{ij}^l equal 0.

Using many of the same values from (4), we can model a standard, single-radio flock of n vehicles for comparison. For this equation, the nodes only use long-range radios to transmit to a ground station. These long-range radios are held in an idle state when not in use to ensure constant communication. Solving again for the total energy of the flock P_f^*

$$P_f^* = \sum_{i=1}^{n} \left(D_{ij}^l \cdot P_t^{*l} - D_{ij}^l \cdot P_{\text{tdl}}^{*l}\right) + n \cdot P_{\text{tdl}}^{*l}. \tag{5}$$

Using (4) and (5), we can simulate the power efficiency improvements of a flock of dual-radio AMP autopilots compared to a standard single-radio flock (see Fig. 8), where each node is downlinking the same amount of data (i.e., $D_{ij}^s = D_{ij}^l$ for all i). Our nondimensional reference value P_c is assigned the CYRF's transmit power of 36.75 mA. Then, using values from the CYRF and XBee datasheets [35], [36], Tables I and II, we can assign our power values to $P_t^{*s} = 1$, $P_t^{*l} = 6.323$,

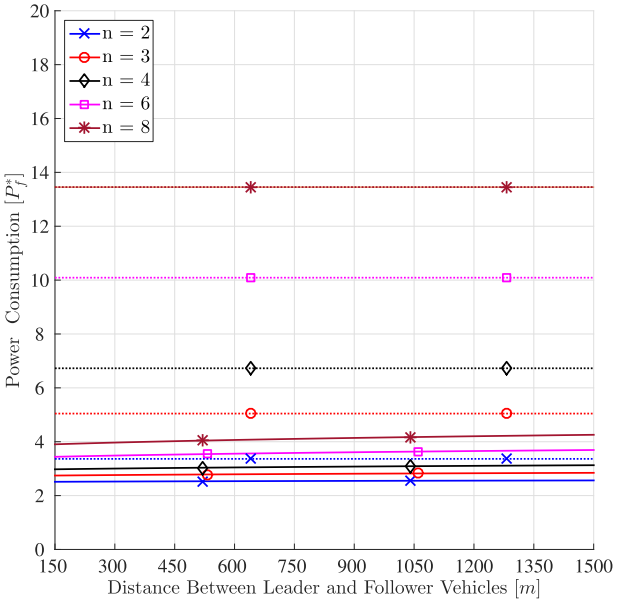

Fig. 9. Simulated power consumption of a flock of AMP autopilots using the dual-radio flock configuration (solid line) and a standard single-radio configuration (dotted line) as the distance between the leader and each of one or more follower vehicles changes. Transmit power is based on target distance, distance to the ground station is 1600 m for all single-radio vehicles and the dual-radio leader, and data rates D_{ij}^s and D_{ij}^l are set to 2.56%. Several cases are shown.

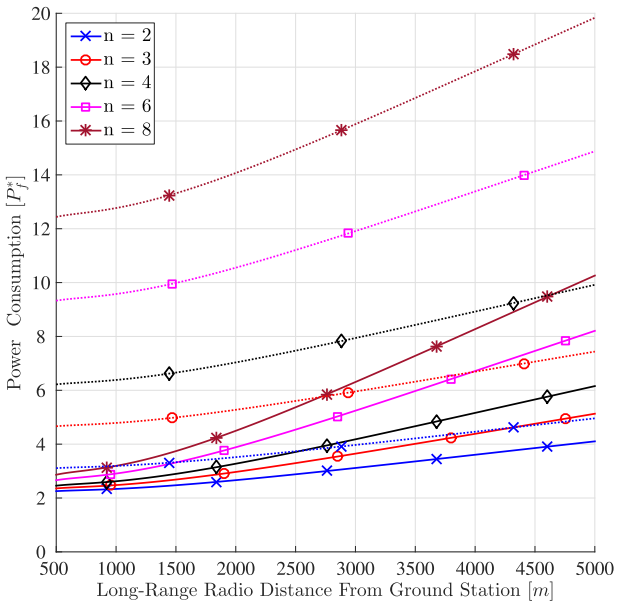

Fig. 10. Simulated power consumption of a flock of AMP autopilots using the dual-radio flock configuration (solid line) and a standard single-radio configuration (dotted line) as the distance between the long-range XBee radio of the dual-radio leader and single-radio vehicles and the ground station changes. Transmit power is based on target distance, distance between the leader and each of one or more followers is 100 m, and data rates D_{ij}^s and D_{ij}^l are set to 2.56%. Several cases are shown.

$P_r^{*s} = 0.647$, $P_r^{*l} = 1.618$, $P_{\text{tdl}}^{*s} = 0.029$, $P_{\text{rdl}}^{*s} = 0.647$, and $P_{\text{tdl}}^{*l} = P_{\text{rdl}}^{*l} = 1.618$.

In Figs. 9–11, we simulate the power efficiency of a dual-radio and standard-radio flock as functions of distance and carrier frequency by using (1) and (3). As previously reported, CYRF values for (1) are as follows: -97 dBm for P_r, 125 mm for λ,

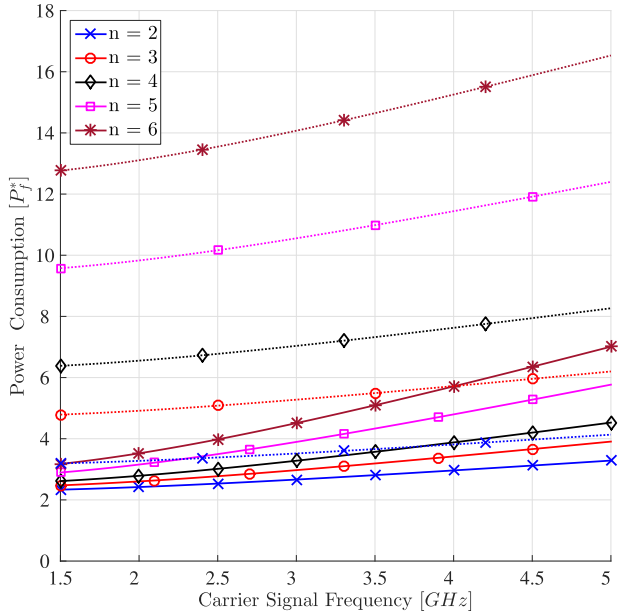

Fig. 11. Simulated power consumption of a flock of AMP autopilots using the dual-radio flock configuration (solid line) and a standard single-radio configuration (dotted line) as the carrier frequency changes. Transmit power is based on target distance and carrier frequency, distance to the ground station is 1600 m for all single-radio vehicles and the dual-radio leader, distance between the leader and each of one or more followers is 100 m, and data rates D_{ij}^s and D_{ij}^l are set to 2.56%. Several cases are shown.

and 3 dBi for D_r and D_t. XBee values for the same equation are as follows: -100 for P_r, 125 mm for λ, and 1.5 dBi for D_r and D_t. Both radios are assigned a fade margin F of 20 dBm.

To estimate realistic transmit power values from the ideal values given by (1), we use the model from (3). For the CYRF, values are assigned as $C_1 = 0.0010972$, $C_2 = 0.073221$, $C_3 = 1.6$, and $C_4 = 93.423$ with an R^2 value (variance of actual data from the model) of 0.988. This fitted model was generated using values from Table I and is shown in Fig. 12. For the XBee, $C_1 = 0.20562$, $C_2 = -8.1087$, $C_3 = 114.07$, and $C_4 = -1350$, with an R^2 value of 1. XBee values were generated using Table II and are shown in Fig. 13.

Analyzing the simulation from Fig. 8, we see that in scenarios where D_{ij}^s and D_{ij}^l values approach 0, that is, when a very small percentage of time is spent transmitting, the performance of the dual-radio configuration is largely determined by the ratio of P_{tdl}^{*l} to P_{tdl}^{*s}, with larger ratios granting increased energy savings. This can be seen where the dual-radio flock simulations appear to converge, but are actually separated by their short-range transmit idle value P_{tdl}^{*s}, increasing with each additional follower vehicle, n, whereas the standard-radio flock simulations are separated by greater consumption values due to the larger value of P_{tdl}^{*l}. The P_{tdl}^{*l} to P_{tdl}^{*s} ratio still dominates as $\sum_{i=1}^{n-1} D_{ij}^s$ and $\sum_{i=1}^{n} D_{ij}^l$ approach 1, but now the value of P_t^{*s} significantly influences power savings, with higher values diminishing flock energy efficiency.

Additionally, in most situations, performance of the flock improves as n increases compared to a standard flock as the dual-radio flock only increases power usage by P_{tdl}^{*s}, whereas the standard flock increases power usage by the larger P_{tdl}^{*l} value. However, one of the limitations highlighted by this model is that

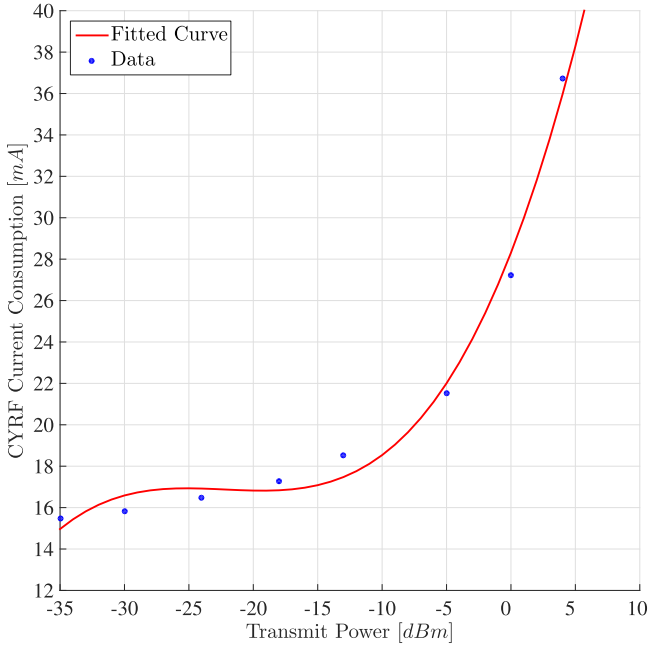

Fig. 12. CYRF transmission power model, fitted using a non-linear, least squares method with data from Table I.

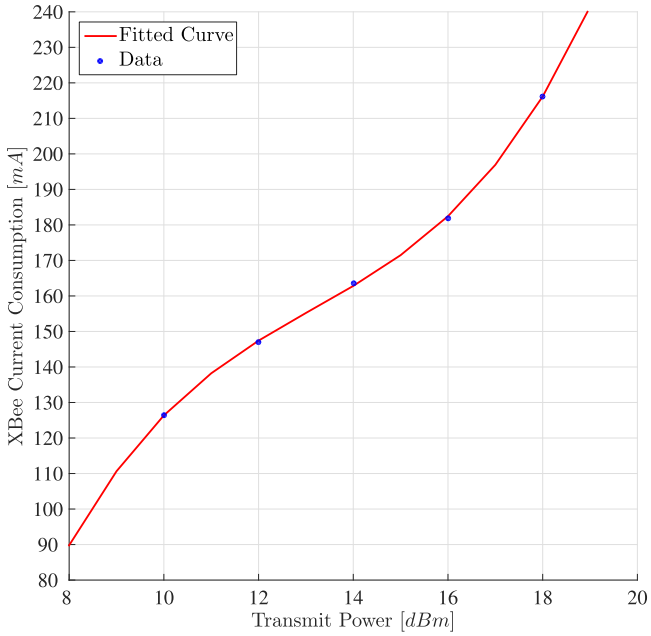

Fig. 13. XBee transmission power model, fitted using a non-linear, least squares method with data from Table II.

users must ensure that the data rates of the leader's short- and long-range radios are sufficient to support the communication needs of the flock. This is essentially due to the limitation that $\sum_{i=1}^{n} D_{ij}^{s}$ and $\sum_{i=1}^{n} D_{ij}^{l}$ must be ≤ 1.

From Figs. 9–11, we can observe how the distance to a transmit target and the carrier frequency affect our flock performance. Intersecting lines in these figures indicate when a standard-radio configuration becomes more power efficient than a dual-radio configuration. In Fig. 9, we see that as the follower vehicle(s) in a dual-radio flock increase their distance from the flock leader, the power efficiency of the flock decreases due to the increased transmit power required by the radio to reach its target, though this increase is only slight. In contrast, Fig. 10 demonstrates how, for flocks whose members are a constant distance apart from one another, increasing distance from the ground station negatively affects power consumption to a greater extent. Again, this is due to the increased transmit power required by the long-range radio to reach its target, which is much larger for distances of this size. Finally, Fig. 11 shows that as the carrier frequency of a signal increases, power efficiency decreases, due to the increased transmit power required to overcome the large attenuation of high-frequency signals.

This dual-radio model makes a number of assumptions. All vehicles within each flock are assumed to be within short-range radio distance of the leader. For simplicity, we do not account for packet loss and assume that radio interference is negligible. We consider crosstalk reception between radios to be insignificant as the nodes of the flock are assumed to be communicating synchronously, so that only one radio is communicating with the leader at any time. Energy consumption of radios in a sleep state is generally two or more orders of magnitude lower than standard communication states, so we assume this is zero. For Figs. 9–11, we assume that the transmit power of the radios automatically adjusts as needed based on transmit distance, that is, the radios have adaptive power control. We also assume a larger, more granular dynamic range of transmit powers than the CYRF and XBee are capable, so as to illustrate how power consumption may change across distances.

V. Flight Experiment

Here we report the results from two of the multiple flight tests that were performed to validate our dual-radio flock model. Experiments were conducted in an open field, without trees or other structures blocking the communication path between the vehicles and the ground station, using two of our Delta Wing platforms (see Fig. 3), each outfitted with an AMP autopilot. Vehicles were hand launched one at a time and flown by a pilot. Once stable flight was achieved, a loiter circle was assigned to each aircraft and the autopilot was enabled. When both MAVs were successfully tracking their loiter circles, the tests started.

The first test took place on a clear day with low winds of about 1–2 km/h and was used as a single-radio benchmark flight. Two vehicles were flown, each transmitting about 800 b of data per second (out of the max transmit rate of 250,000 b/s) to the ground station over XBee radio. The transmitted data consisted of power, location, and rotation information for the vehicle. The two aircrafts followed loiter circles with radii of 70 m. From their centers of loiter, vehicle 1 was offset 20 m southeast of vehicle 2. Vehicle 1 loitered at an altitude of 100 m, whereas vehicle 2 loitered at an altitude of 110 m. Fig. 14(a) shows the flight paths for the two vehicles and Fig. 14(b) shows the power consumption for vehicle 1, vehicle 2, the combined flock, and the standard-radio flock simulation for two vehicles.

The second test was used to validate the dual-radio flock configuration. This test took place on a clear day, with moderate winds of about 8 km/h. As this was only a two vehicle flock, the status of leader was assigned to the vehicle closer to the

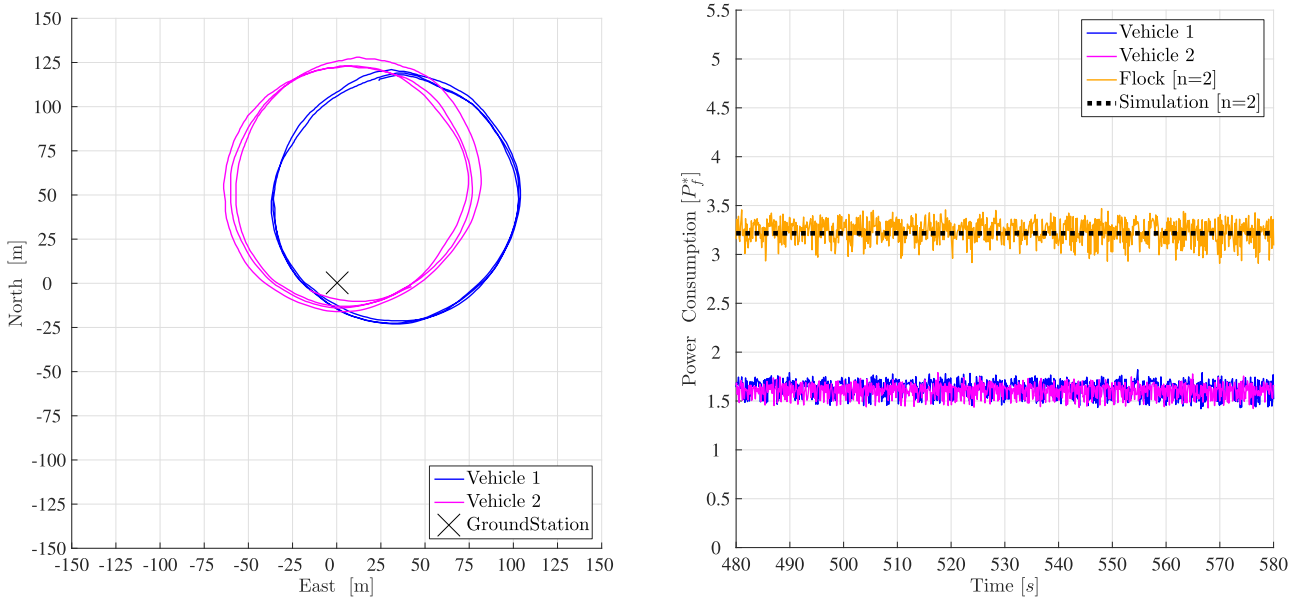

(a) (b)

Fig. 14. Representations of (a) the flight trajectory of the two Delta Wing platforms outfitted with AMP boards compared with (b) the power usage of the vehicles during this standard-radio flight. For (b), power values represent power consumption from just the radio subsystems operating at max transmit power and are nondimensionalized by assigning the reference value P_c to the CYRF's max transmit power of 36.75 mA. The standard-radio flock simulation result ($n = 2$) from (5) is plotted as a value of 3.216, compared to the mean flock value of 3.235.

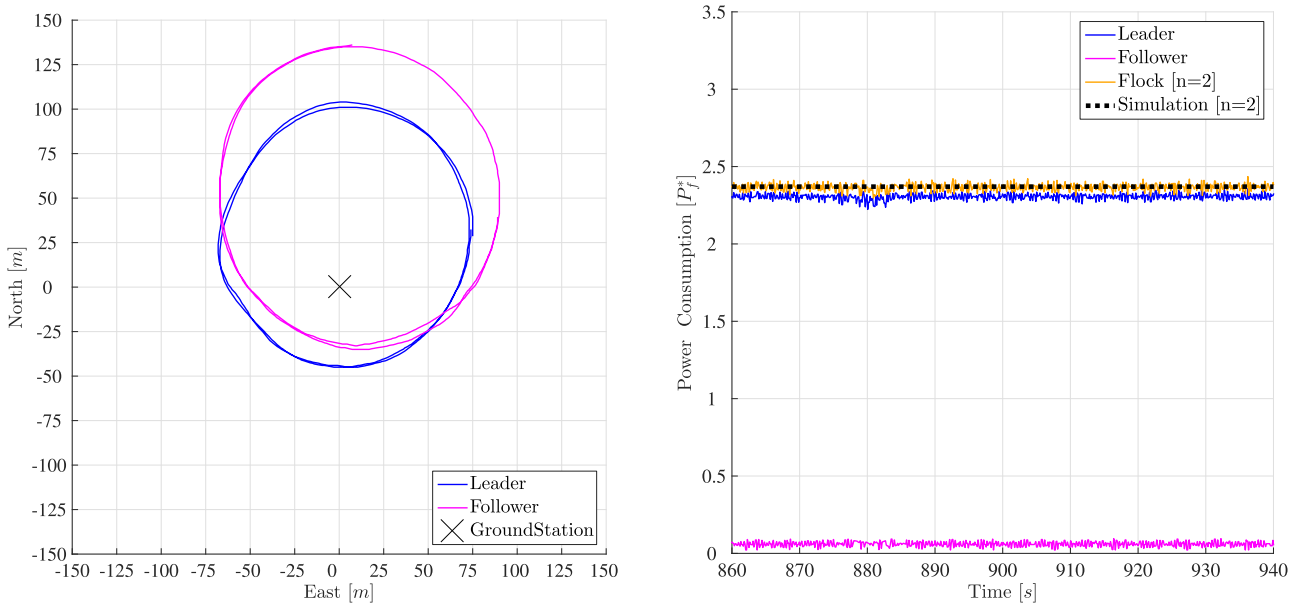

(a) (b)

Fig. 15. Representations of (a) the flight trajectory of the two Delta Wing platforms outfitted with AMP boards compared with (b) the power usage of the vehicles during this dual-radio configuration flight. For (b), power values represent power consumption from just the radio subsystems operating at max transmit power and are nondimensionalized by assigning the reference value P_c to the CYRF's transmit power of 36.75 mA. The dual-radio flock simulation result ($n = 2$) from (4) is plotted as a value of 2.370, compared to the mean flock value of 2.350. Values in this plot appear less noisy than those in Fig. 14(b) as the INA226 power sensor was performing a higher rate of self-averaging (256 averaged samples compared to 64).

ground station when the test began. Again, both vehicles transmitted 800 b of data per second, consisting of power, location, and rotation information for the vehicle. But for this flight, following the dual-radio model, the follower vehicle transmitted to the leader over short-range CYRF radio, and the leader relayed both its and the follower's data to the ground station via long-range XBee radio. The leader vehicle loitered with a radius of about 70 m, whereas the follower vehicle loitered with a radius of 85 m. The two vehicles were offset 20 m longitudinally from their centers of loiter. The leader loitered at an altitude of 100 m, whereas the follower loitered at an altitude of 110 m. Fig. 15(a) shows the flight paths for the two vehicles

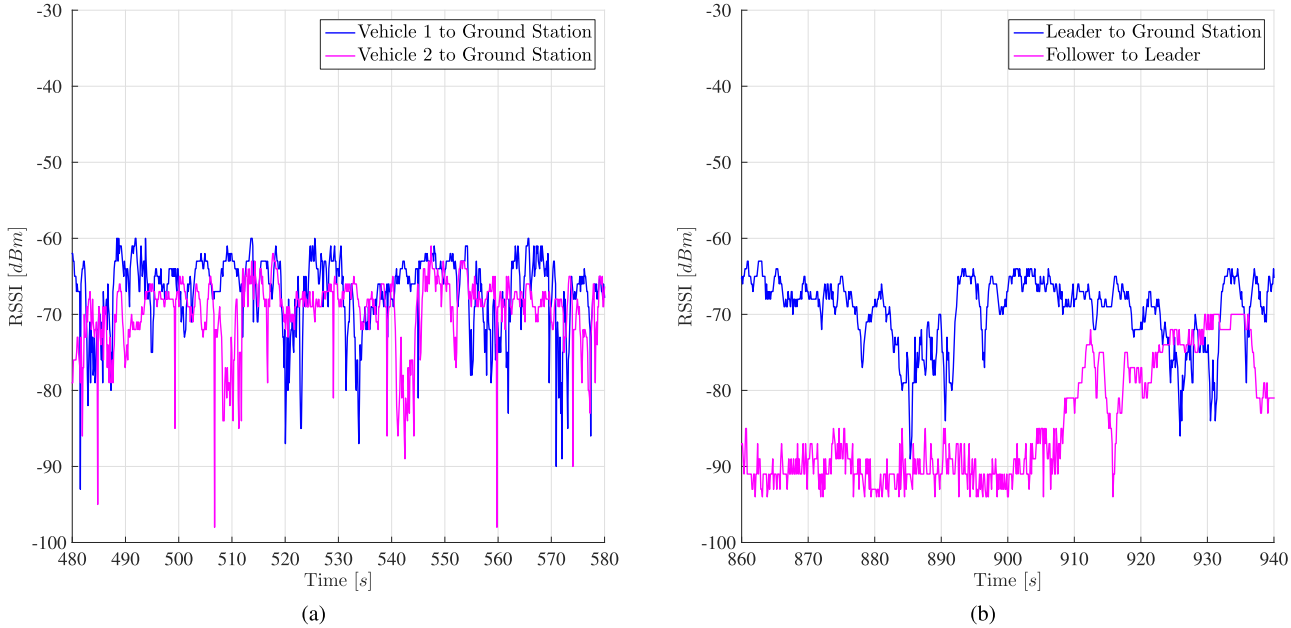

Fig. 16. Representations of (a) the RSSI between the vehicles and the ground station during the segment of the standard radio flight shown in Fig. 14 and (b) the RSSI between the leader and ground station and the follower and leader during the segment of the dual radio flight shown in Fig. 15. RSSI values received by the CYRF are lower resolution than those received by the XBee. Higher values are better.

and Fig. 15(b) shows the power consumption for the leader, follower, the combined flock, and the dual-radio flock simulation for two vehicles.

Fig. 16 shows the received signal strength indicator (RSSI) between the vehicles and ground station during the previously mentioned flights. RSSI is a good indicator of the strength of a received signal and the quality of a communication link. A periodic improvement and degradation of the signal quality can be observed from both parts of Fig. 16. This is likely due to the periodic nature of the vehicles flying near to, and then far from, the ground station, as the flight paths from Figs. 14 and 15 show. Another observation is that the RSSI link between the follower and leader, the intervehicle link maintained by the CYRF, is noticeably worse than that of the link between the vehicles and the ground station, the long-range link maintained by the XBee. We suspect two major reasons for this. The first is due to the CYRF6936's much lower transmit power of 4 dBm compared to the XBee Pro's transmit power of 18 dBm. The second reason may be because the CYRF6936's sensitive antenna circuits were hand-soldered, resulting in lower quality signal transmission and reception, whereas the XBees used were professionally manufactured.

To reduce interference, members of the flock communicate synchronously with the leader, and the CYRF and XBee radios communicate on different channels of the 2.4-GHz band. As the flock grows, we expect the synchronous communication to keep crosstalk interference between members of the flock to a minimum, though this may result in increased data latency. Additionally, as the flock grows, the issue of flock members physically obstructing one another's wireless signals increases. These problems could be alleviated by either splitting a large flock into smaller groups based on some optimal flock size, or by potentially increasing the number of leaders within a flock. With regard to the problem of physical obstruction, flocking formation and organization control could be used to mitigate this issue. Additionally, these tests were performed in a rural environment. Here, congestion from other wireless signals was kept to a minimum and physical obstructions, such as buildings or trees (which could obstruct line-of-sight radios, such as the XBee and CYRF) were avoided. We hope to further investigate and address these issues and fly in more urban environments in our future work.

This dual-radio configuration uses a leader/follower hierarchy to improve flexibility and reduce the overall cost of communication within and between flocks. Other flock models have used hierarchical or flat agent-to-agent structures for a number of benefits [41], [42]. Implementing a hierarchical flock model can reduce the total amount of communication required between members, as followers only need communicate with a leader [43], [44]. Furthermore, hierarchies simplify formation control and member cohesion within a group of vehicles [43], [45], [46]. Other flock models use flat, egalitarian structures, which commonly operate around the concept of agents cooperating with their nearby neighbors [8], [47], [48]. Furthermore, some models switch between these two structures in an attempt to best respond to the current situation [44].

From these flights, we can see that the dual-radio configuration improved flock radio power efficiency by about 37%. These power savings also appear to align with our 2.56% D_{ij}^{s} and D_{ij}^{l} values from the model simulation shown in Fig. 8. Additionally, the leader and follower managed to maintain a reasonably stable connection, despite at times being separated by over 100 m, the maximum range listed for the CYRF6936. Based on these results, we believe that this dual-radio model could be useful for determining the performance gains of other dual-radio autopilot configurations used on MAVs or UAVs.

VI. Conclusion

We have proposed a flexible, dual-radio autopilot flock configuration. This configuration is based on the concept that by handling interflock communication using low-power, short-range radios and adopting a leader/follower hierarchy—in which an elected leader node relays all flock transmissions to one or more ground stations over long-range radio—the remaining flock may conserve power by placing their long-range radios in a low-power sleep state. This is compared to a standard single-radio autopilot flock, in which each autopilot must idle their radio to ensure constant communication, a state that can rapidly drain a battery. Additionally, the diversity offered by the dual-radio autopilot provides for inherent redundancy in communication, adaptability when communicating with multiple targets at varying distances, and improved throughput by aggregating radio communication.

A new dual-radio ground station platform called the SuperBoard was also designed and presented. This ground station platform allows us to facilitate communication over both radios through a single interface and preprocess outgoing and incoming data through the onboard processor.

We created a mathematical model and simulations representing and comparing our dual-radio configuration against a standard, single-radio flock. Simulations for a variety of flock sizes, distances, and data rates were presented and discussed.

Successful multi-vehicle flight tests were performed using our group's AMP autopilot [19] to compare the power usage of a single-radio autopilot flock to the proposed dual-radio flock. From our flight results, the dual-radio flock configuration showed a 37% improvement in power savings compared to a standard, single-radio flock of the same size. These flights also demonstrated the accuracy of our model, which was within 1% of our actual radio values. These power savings only grow with the size of the flock, where according to our model, flocks as large as six vehicles can see improvements of over 200% compared with a standard-radio flock of the same size.

While the power savings of this configuration are diminished when compared to single-radio flocks using more expensive radios with lower idle and transmit powers, for those who wish to use economical radios to keep their MAV flocks affordable, flexible, and power efficient, the dual-radio flock is a highly viable option.

Subsequent work for our dual-radio autopilot may include optimizing the transmit power of individual radios to improve power usage, routing data through more than one leader node to improve bandwidth and reduce latency, and introducing heterogeneous radio configurations within the flock and assigning leader nodes based on radio capabilities. Additionally, we hope to perform tests in more urban environments in the hopes of observing how this dual-radio configuration performs with additional wireless interference and physical obstructions.

Acknowledgment

The authors would like to thank M. Silic and D. Tansel for their assistance with performing tests and designing hardware.

References

[1] A. Malaver, N. Motta, P. Corke, and F. Gonzalez, "Development and integration of a solar powered unmanned aerial vehicle and a wireless sensor network to monitor greenhouse gases," *Sensors*, vol. 15, no. 2, pp. 4072–4096, 2015. [Online]. Available: http://www.mdpi.com/1424-8220/15/2/4072/htm

[2] D. Lipinski and K. Mohseni, "Micro/miniature aerial vehicle guidance for hurricane research," *IEEE Syst. J.*, vol. 10, no. 3, pp. 1263–1270, Sep. 2015.

[3] L. Peng, D. Lipinski, and K. Mohseni, "Dynamic data driven application system for plume estimation using UAVs," *J. Intell. Robot. Syst.*, vol. 74, no. 1–2, pp. 421–436, 2014. [Online]. Available: http://dx.doi.org/10.1007/s10846-013-9964-x

[4] P.-V. Mekikis, A. Antonopoulos, E. Kartsakli, L. Alonso, and C. Verikoukis, "Communication recovery with emergency aerial networks," *IEEE Trans. Consum. Electron.*, vol. 63, no. 3, pp. 291–299, Aug. 2017.

[5] P.-V. Mekikis, E. Kartsakli, L. Alonso, and C. Verikoukis, "Flexible aerial relay nodes for communication recovery and D2D relaying," in *Proc. IEEE Global Conf. Consum. Electron.*, Kyoto, Japan, Oct. 2016, pp. 1–2.

[6] S. Diamond and M. Ceruti, "Application of wireless sensor network to military information integration," in *Proc. Int. Conf. Ind. Inform.*, Vienna, Austria, Jun. 2007, pp. 317–322. [Online]. Available: http://ieeexplore.ieee.org/abstract/document/4384776/

[7] S. Hayat, E. Yanmaz, and R. Muzaffar, "Survey on unmanned aerial vehicle networks for civil applications: A communications viewpoint," *IEEE Commun. Surveys Tut.*, vol. 18, no. 4, pp. 2624–2661, Oct.–Dec. 2016.

[8] A. Shaw and K. Mohseni, "A fluid dynamic based coordination of a wireless sensor network of unmanned aerial vehicles: 3-D simulation and wireless communication characterization," *IEEE Sensors J., Special Issue Cognitive Sensor Netw.*, vol. 11, no. 3, pp. 722–736, Mar. 2011. [Online]. Available: http://dx.doi.org/10.1109/JSEN.2010.2064294

[9] S. Ravela, I. Sleder, and J. Salas, "Mapping coherent atmospheric structures with small unmanned aircraft systems," in *Proc. Guid., Navig., Control Conf.*, Boston, MA, USA, Aug. 2013, pp. 1–11.

[10] M. Saska, J. Langr, and L. Přeučil, "Plume tracking by a self-stabilized group of micro aerial vehicles," in *Proc. Int. Workshop Model. Simul. Auton Syst.*, Rome, Italy, Jun. 2014, pp. 44–55.

[11] D. A. Lawrence and B. B. Balsley, "High-resolution atmospheric sensing of multiple atmospheric variables using the datahawk small airborne measurement system," *J. Atmos. Ocean. Technol.*, vol. 30, no. 10, pp. 2352–2366, 2013.

[12] A. S. Tanenbaum and D. J. Wetherall, *Computer Networks*, 4th ed. Upper Saddle River, NJ, USA: Prentice-Hall, 2003.

[13] E. H. Ong, J. Kneckt, O. Alanen, Z. Chang, T. Huovinen, and T. Nihtilä, "IEEE 802.11 AC: Enhancements for very high throughput WLANs," in *Proc. Int. Symp. Pers. Indoor Mobile Radio Commun.*, Toronto, ON, Canada, Sep. 2011, pp. 849–853.

[14] L. Casals, B. Mir, R. Vidal, and C. Gomez, "Modeling the energy performance of LoRaWAN," *Sensors*, vol. 17, no. 10, 2017, Art. no. E2364.

[15] Z. Song and K. Mohseni, "Hierarchical underwater localization in dominating background flow fields," in *Proc. IEEE/RSJ Int. Conf. Intell. Robots Syst.*, Tokyo, Japan, Nov. 2013, pp. 3356–3361. [Online]. Available: http://dx.doi.org/10.1109/IROS.2013.6696834

[16] Z. Song and K. Mohseni, "FACON: A flow-aided cooperative navigation scheme," in *Proc. IEEE/RSJ Int. Conf. Intell. Robots Syst.*, Vancouver, BC, Canada, Sep. 2017, pp. 6251–6256.

[17] Z. Song, D. Lipinski, and K. Mohseni, "Multi-vehicle cooperation and nearly fuel-optimal flock guidance in strong background flows," *Ocean Eng.*, vol. 141, pp. 388–404, 2017. [Online]. Available: https://doi.org/10.1016/j.oceaneng.2017.06.024

[18] Y. Zeng, R. Zhang, and T. Lim, "Wireless communications with unmanned aerial vehicles: Opportunities and challenges," *IEEE Commun. Mag.*, vol. 54, no. 5, pp. 36–42, May 2016. [Online]. Available: http://ieeexplore.ieee.org/abstract/document/7470933/

[19] A. Bingler and K. Mohseni, "Dual radio autopilot system for lightweight, swarming micro/miniature aerial vehicles," *J. Aerosp. Inf. Syst.*, vol. 14, no. 5, pp. 293–305, 2017. [Online]. Available: https://doi.org/10.2514/1.I010445

[20] C. Wan, S. Eisenman, A. Campbell, and J. Crowcroft, "Siphon: Overload traffic management using multi-radio virtual sinks in sensor networks," in *Proc. Int. Conf. Embedded Netw. Sensor Syst.*, San Diego, CA, USA, Nov. 2005, pp. 116–129. [Online]. Available: https://dl.acm.org/citation.cfm?id=1098931

[21] S. Ji, Z. Cai, Y. Li, and X. Jia, "Continuous data collection capacity of dual-radio multichannel wireless sensor networks," *IEEE Trans. Parallel Distrib. Syst.*, vol. 23, no. 10, pp. 1844–1855, Oct. 2012. [Online]. Available: http://ieeexplore.ieee.org/document/6095527/

[22] Y. Ding, K. Pongaliur, and L. Xiao, "Channel allocation and routing in hybrid multichannel multiradio wireless mesh networks," *IEEE Trans. Mobile Comput.*, vol. 12, no. 2, pp. 206–218, Feb. 2013.

[23] F. Z. Djiroun and D. Djenouri, "MAC protocols with wake-up radio for wireless sensor networks: A review," *IEEE Commun. Surveys Tut.*, vol. 19, no. 1, pp. 587–618, Jan.–Mar. 2017.

[24] A. A. Islam, M. S. Hossain, V. Raghunathan, and Y. C. Hu, "Backpacking: Energy-efficient deployment of heterogeneous radios in multi-radio high-data-rate wireless sensor networks," *IEEE Access*, vol. 2, pp. 1281–1306, 2014.

[25] A. Yadav, G. I. Tsiropoulos, and O. A. Dobre, "Full-duplex communications: performance in ultradense mm-wave small-cell wireless networks," *IEEE Veh. Technol. Mag.*, vol. 13, no. 2, pp. 40–47, Jun. 2018.

[26] R. Jurdak, K. Klues, B. Kusy, C. Richter, K. Langendoen, and M. Brunig, "Opal: A multiradio platform for high throughput wireless sensor networks," *IEEE Embedded Syst. Lett.*, vol. 3, no. 4, pp. 121–124, 2011. [Online]. Available: http://ieeexplore.ieee.org/document/6086565/

[27] Y. Agarwal, R. Chandra, A. Wolman, P. Bahl, K. Chin, and R. Gupta, "Wireless wakeups revisited: Energy management for VOIP over Wi-Fi smartphones," in *Proc. Int. Conf. Mobile Syst., Appl. Serv.*, San Juan, PR, USA, Jun. 2007, pp. 179–191. [Online]. Available: https://dl.acm.org/citation.cfm?id=1247682

[28] H. Karvonen, J. Petajajarvi, V. Niemela, M. Hamalainen, J. Iinatti, and R. Kohno, "Energy efficient UWB-WUR dual-radio solution for WBANs," in *Proc. Int. Symp. Med. Inf. Commun. Technol.*, Lisbon, Portugal, Feb. 2017, pp. 64–68.

[29] F. Sutton and L. Thiele, "Wake-up flooding: An asynchronous network flooding primitive," in *Proc. Int. Conf. Inf. Process. Sensor Netw.*, Seattle, WA, USA, Apr. 2015, pp. 360–361.

[30] Y. Agarwal, T. Pering, R. Want, and R. Gupta, "SwitchR: Reducing system power consumption in a multi-client, multi-radio environment," in *Proc. Int. Symp. Wearable Comput.*, Pittsburgh, PA, USA, Sep./Oct. 2008, pp. 99–102. [Online]. Available: http://ieeexplore.ieee.org/document/4911593/

[31] B.-H. Liu, V.-T. Pham, and N.-T. Nguyen, "A virtual backbone construction heuristic for maximizing the lifetime of dual-radio wireless sensor networks," in *Proc. Int. Conf. Intell. Inf. Hiding Multimedia Signal Process.*, Adelaide, SA, Australia, Sep. 2015, pp. 64–67.

[32] F. Kauer, E. Kallias, and V. Turau, "A dual-radio approach for reliable emergency signaling in critical infrastucture assets with large wireless networks," *Int. J. Crit. Infrastruct. Protection*, vol. 21, pp. 33–46, 2018. [Online]. Available: https://doi.org/10.1016/j.ijcip.2018.02.002

[33] B. Hodgkinson, D. Lipinski, L. Peng, and K. Mohseni, "High resolution atmospheric sensing using UAV swarms," in *Proc. Int. Symp. Distrib. Auton. Robot. Syst.*, Daejeon, South Korea, Nov. 2014, pp. 31–45. [Online]. Available: http://dx.doi.org/10.1007/978-3-642-55146-8

[34] Y. Mitikiri and K. Mohseni, "Attitude control of micro/mini aerial vehicles and estimation of aerodynamic angles formulated as parametric uncertainties," *IEEE Robot. Autom. Lett.*, vol. 3, no. 3, pp. 2063–2070, Jul. 2018.

[35] *WirelessUSB LP 2.4 GHz Radio SoC*, Cypress, San Jose, CA, USA, Rev. K, Apr. 2014.

[36] *XBee /XBee-PRO RF Modules*, Digi, Minnetonka, MN, USA, Sep. 2009.

[37] R. Johnson and H. Jasik, *Antenna Engineering Handbook*, 2nd ed. New York, NY, USA: McGraw-Hill, 1984.

[38] J. Unger, *Deploying License-Free Wireless Wide-Area Networks*. Indianapolis, IN, USA: Cisco Press, 2003.

[39] D. Lymberopoulos and A. Savvides, "XYZ: A motion-enabled, power aware sensor node platform for distributed sensor network applications," in *Proc. Int. Symp. Inf. Process. Sensor Netw*, Los Angeles, CA, USA, Apr. 2005, paper 63. [Online]. Available: https://dl.acm.org/citation.cfm?id=1147762

[40] A. Jensen, M. Lauridsen, P. Mogensen, T. Sørensen, and P. Jensen, "LTE UE power consumption model: For system level energy and performance optimization," in *Proc. Veh. Technol. Conf.*, Quebec City, QC, Canada, Sep. 2012, pp. 1–5. [Online]. Available: http://ieeexplore.ieee.org/abstract/document/6399281/

[41] V. Chepizhenko and O. Aliakin, "Analysis of unmanned aerial vehicle formation flight control methods," *Proc. Nat. Aviation Univ.*, Kiev, Ukraine, vol. 3, pp. 22–17, 2015.

[42] I. Maza, A. Ollero, E. Casado, and D. Scarlatti, "Classification of multi-UAV architectures," in *Handbook of Unmanned Aerial Vehicles*, K. Valavanis and G. Vachtsevanos, Eds. New York City, NY, USA: Springer, 2015, pp. 953–975.

[43] L. He, P. Bai, X. Liang, J. Zhang, and W. Wang, "Feedback formation control of UAV swarm with multiple implicit leaders," *Aerosp. Sci. Technol.*, vol. 72, pp. 327–334, 2018. [Online]. Available: https://doi.org/10.1016/j.ast.2017.11.020

[44] H. Qiu and H. Duan, "Pigeon interaction mode switch-based UAV distributed flocking control under obstacle environments," *ISA Trans.*, vol. 71, pp. 93–102, 2017. [Online]. Available: https://doi.org/10.1016/j.isatra.2017.06.016

[45] C. Kownacki and D. Ołdziej, "Fixed-wing UAVs flock control through cohesion and repulsion behaviours combined with a leadership," *Int. J. Adv. Robot. Syst.*, vol. 13, no. 1, pp. 1–36, 2016. [Online]. Available: https://doi.org/10.5772/62249

[46] L. Hardy, "Implementing cooperative behavior & control using open source technology across heterogeneous vehicles," Master's thesis, Air Force Inst. Technol., Wright-Patterson Air Force Base Ohio, Graduate School of Engineering and Management, OH, USA, 2015.

[47] S. Spanogianopoulos, Q. Zhang, and S. Spurgeon, "Fast formation of swarm of UAVs in congested urban environment," *IFAC-PapersOnLine*, vol. 50, no. 1, pp. 8031–8036, 2017. [Online]. Available: https://doi.org/10.1016/j.ifacol.2017.08.1228

[48] M. B. Silic, Z. Song, and K. Mohseni, "Anisotropic flocking control of distributed multi-agent systems using fluid abstraction," in *Proc. AIAA Inf. Syst.*, Kissimmee, FL, USA, Jan. 2018, pp. 2018–2262. [Online]. Available: https://doi.org/10.2514/6.2018-2262

Andrew Bingler received the B.S. degree in computer engineering and the M.S. degree in electrical engineering from the University of Florida, Gainesville, FL, USA, in 2015 and 2017, respectively.

He has been with the Institute for Networked Autonomous Systems, since 2014 and a Graduate Researcher with the Department of Electrical and Computer Engineering, University of Florida, Gainesville, FL, USA, since 2015.

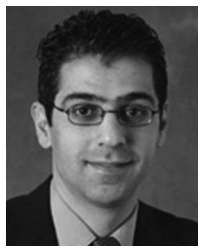

Kamran Mohseni (M'95) received the Ph.D. degree in mechanical engineering from the California Institute of Technology (Caltech), Pasadena, CA, USA, in 2000.

After a year as a Postdoc in control and dynamical systems at Caltech, he joined the University of Colorado at Boulder, Boulder, CO, USA, as an Assistant and then Associate Professor with the Department of Aerospace Engineering Sciences before moving to Florida as the W.P. Bushnell Endowed Chair with both the Mechanical and Aerospace Engineering Department and the Electrical and Computer Engineering Department, University of Florida, Gainesville, FL, USA. He is the Director of the Institute for Networked Autonomous Systems.

Dr. Mohseni is a member of the American Society of Mechanical Engineers, the American Physical Society, and the Society for Industrial and Applied Mathematics, and an Associate Fellow of the American Institute of Aeronautics and Astronautics.